

MASS LOSS BY X-RAY WINDS FROM ACTIVE GALACTIC NUCLEI

DORON CHELOUCHE¹

Draft version September 14, 2017

ABSTRACT

We consider a sample of type-I active galactic nuclei (AGN) that were observed by *Chandra/HETG* and resulted in high signal-to-noise grating spectra, which we study in detail. All objects show signatures for very high ionization outflows. Using a novel scheme to model the physics and spectral signatures of gaseous winds from these objects, we are able to estimate the mass loss rates and kinetic luminosities associated with the highly ionized gas and investigate its physical properties. Our conclusions are as follows: 1) There is a strong indication that the outflowing gas in those objects is multi-phase with similar kinematics for the different phases. 2) The X-ray spectrum is consistent with such flows being thermally driven from \sim pc scales, and are therefore unlikely to be associated with the inner accretion disk. 3) The underlying X-ray spectrum consists of a hard X-ray powerlaw which is similar for all objects shining below their Eddington rate and a soft excess whose contribution becomes more prominent for objects shining close to their Eddington limit. 4) The physical properties of the outflow are similar in all cases and a coherent picture emerges concerning its physical properties. 5) The deduced mass loss rates are, roughly, of the order of the mass accretion rate in those objects so that the kinetic luminosity carried by such winds is only a tiny fraction ($\ll 1\%$) of the bolometric luminosity. We discuss the implications of our results for AGN structure and AGN interaction with the environment.

Subject headings: acceleration of particles — ISM: jets and outflows — galaxies: Seyfert — quasars: absorption lines — X-rays: individual (NGC 3783, NGC 5548, NGC 7469, NGC 4151, MCG-6-30-15)

1. INTRODUCTION

Recent *Chandra* and *XMM* grating observations of type-I (broad emission lines) active galactic nuclei (AGN) show the presence of highly ionized gas (HIG) outflowing from the centers of many objects (e.g., Kaastra et al. 2000, Kaspi et al. 2001, Pounds et al. 2003, McKernan et al. 2007). This suggests that HIG may play an important role in AGN physics and so must be included in future unification schemes (e.g., Elvis 2000). Currently, however, little is known with confidence about the physical properties of this component and a clear physical picture is yet to emerge. In addition to being important for AGN study, HIG flows carry energy and momentum out from their inner engine to potentially large scales and, as such, may have a profound impact on the environment of quasars, be it their host galaxies or even the intergalactic medium (e.g., Di Matteo et al. 2005, Scannapieco & Oh 2003). Thus, constraining the physical properties of AGN outflows is a fundamental question in AGN physics with great implications for a wide range of astrophysical problems.

Detailed X-ray spectroscopic observations of a few nearby low-luminosity AGN (Seyfert 1 galaxies) indicate that HIG outflows have a stratified ionization structure and that they are located within a parsec or so from the central continuum source (e.g., Blustin et al. 2007, Kaspi & Behar 2006, Kraemer et al. 2005, Krongold et al. 2003, 2009, Netzer et al. 2003, Schulz et al. 2008, Smith et al. 2007, Steenbrugge et al. 2005). The outflowing gas appears to be multiphase with various phases being in a rough pressure equilibrium and lying on the thermally stable parts of the heating-cooling curve (e.g., Chakravorty et al. 2008, Holczer et al. 2007, Netzer et al. 2003). Despite the considerable progress in our phenomenological understanding of HIG flows, their underlying

physics remains elusive. For example, a detailed investigation of the best studied HIG in AGN (the case of NGC 3783) yielded mass loss rates in the range of a few percent to nearly a hundred solar masses per year (e.g., Behar et al. 2003, Blustin et al. 2005, Netzer et al. 2003). Some studies pre-suppose that the mass loss rate is less than or equal to the mass accretion rate (e.g., Steenbrugge et al. 2005) yet it is not clear that this must be the case. Clearly, the current situation is unsatisfactory if we wish to understand the role of HIG flows in the global picture of AGN and assess their effect on the environment of such objects.

Perhaps the main limitation that prevents us from fully understanding the HIG phenomenon in AGN results from model incompleteness: for example, some works dealing with HIG absorption measure the column densities from individual transitions and attempt to estimate the mass loss rate by requiring full volume filling gas, which does not seem to be supported by recent observational and theoretical work; e.g., Arav, Li, & Begelman 1994, Kraemer et al. 2005, Proga et al. 2008). Other works make use of detailed photoionization calculations and spectral modeling to determine the temperature and column density range of the HIG (e.g., Kaspi et al. 2002, Krongold et al. 2003, Netzer et al. 2003, Rózańska et al. 2006). Nevertheless, pure photoionization modelling does not account for the kinematics of the outflow and cannot be used to reveal the location of the gas. This is due to an inherent degeneracy between the density of the photoionized gas and the distance from the ionizing source for a wide range of densities relevant to HIG outflows (see however Rózańska et al. 2008). Limits on the location of the gas may be obtained by studying the reaction of the photo-ionized gas to the varying ionizing flux level of the source, as has been done for the case of NGC 3783 (Netzer et al. 2003, Krongold et al. 2005; see also Chevallier et al. 2007). New numerical schemes that self-consistently model the gas dynamics as well as its thermal

¹ Canadian Institute for Theoretical Astrophysics, University of Toronto, 60 St. George st., Toronto ON M5S 3H8, Canada; doron@cita.utoronto.ca

state were recently calculated by Dorodnitsyn et al. (2008a,b) and their spectral predictions are yet to be compared to observations. Thus, the physics of HIG outflows in AGN and, in particular, the estimates for the mass carried by them are subject to considerable uncertainties.

Recently, Chelouche & Netzer (2005; hereafter CN05) have demonstrated that, by employing a detailed and self-consistent modelling of the dynamics and photoionization properties of the outflowing gas, it may be possible to constrain the mass loss rate to much better precision than before. By applying their model to NGC 3783, they found that the mass loss rate is considerably smaller compared to previous estimates. While their model seems to be consistent with most observational constraints for the case of NGC 3783, it is yet to be confirmed for other AGN. Here we wish to adopt a more general approach and study a sample of X-ray bright, nearby type-I AGN and investigate their properties using a consistent analysis method. Specifically, we wish to test the thermally driven wind model as a possible new ingredient of the AGN structure and do that by considering several objects where such advanced analysis is warranted. Our aim is to gain better physical understanding of the AGN phenomenon as is emerging from high resolution and S/N observations and understand the dynamics of highly ionized gas in those systems. In addition, we wish to quantify the mass loss rate from these objects which have been claimed to have a paramounting effect on the environment of such objects.

In this paper we consider a sample of X-ray bright, nearby type-I AGN (Seyfert 1-1.5 galaxies) for which high quality grating spectra are available and the mass of the central black-hole has been measured. We improve upon the model of CN05 and apply it to study HIG outflows in those objects. The paper is organized as follows: In §2 we present the sample of objects used in this work and discuss their properties. Section 3 outlines the basics of our model and the improvements and generalizations made to the CN05 scheme. Results of our spectral modelling pertaining to individual objects are presented in §4. We discuss the implications of our results for the unification scheme of AGN and AGN interaction with their environment in §5. Summary follows in §6.

2. THE SAMPLE

Our sample was constructed having in mind the Netzer et al. (2003) and CN05 spectral analysis method. This method uses the silicon and sulphur lines near 2 keV to constrain the properties of the ionized outflow over a wide range of ionization levels. This enables one to eliminate many of the uncertainties and degeneracies associated with the intrinsic continuum shape at soft X-rays (e.g., Netzer et al. 2003). Also, the CN05 results suggest that, at least for NGC 3783, most of the mass loss is due to an extremely ionized component of the flow. Such gas is, however, much harder to detect and requires good signal to noise (S/N) and high resolution observations in the hard X-ray band. Currently, these wavelengths are best covered by the *Chandra* gratings (the *XMM/RGS* has negligible effective area shortward of $\sim 12\text{\AA}$). For this reason our sample is essentially flux limited and is restricted to relatively nearby objects that have been observed by the *Chandra* high energy transmission grating (HETG); we note that despite its large effective area, the LETG is not favored for this study due to its very low resolution at short wavelengths (see also §4.1). We have thus searched the *Chandra* archive for bright AGN with long grating exposure times. Our search yielded five objects (including NGC 3783 which is included here only for com-

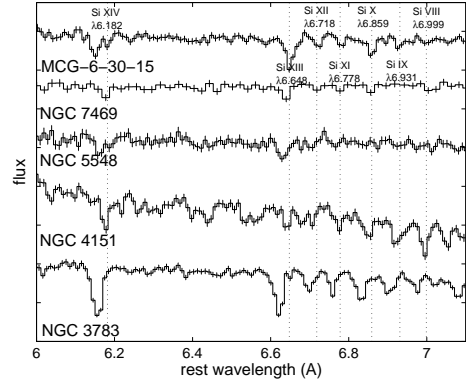


FIG. 1.— The X-ray band containing the inner shell silicon line spectrum for all the objects in our sample. Clear absorption signatures due to highly ionized gas (specifically due to Si XIV $\lambda 6.187$) are evident in all objects regardless of their classification and/or prior evidence for the existence of “warm absorbing” gas (George et al. 1998). Also, the blueshift of the lines with respect to the systemic velocity of the system indicates gas which is outflowing. We note that the spectrum of NGC 7469 is the combined spectrum from two observations (after correcting for the slight difference in flux level) and rebinned to increase the S/N.

pleteness purposes and is discussed in CN05) that are listed in table 1. For each object in our sample we have collected all archived *Chandra/HETG* (and in some cases also LETG) observations and reduced those using CIAO (v3.1) and CALDB (v3.1), using the standard CXC threads. In some case we also analyzed *XMM* data to gain additional information concerning the source although these spectra have not been used to derive the outflow properties. (*XMM* data were reduced using the Science Analysis Software, SAS v.5.3.0 with the standard processing chains. For the detailed spectral analysis (see section 4) we have included only HETG data and, where possible, combined several exposures to increase the S/N, after verifying they have a similar spectrum (see table 1).

Some relevant physical properties for each object in our sample are given in table 1. An important parameter for any dynamical modelling and, in particular, to the CN05 model, is the mass of the central black hole, M_{BH} , assumed to dominate in the inner regions of the AGN (see however Shödel et al. 2003 and Everett & Murray 2007). Thus, it is important that the black hole mass be known to a good precision. Currently, the best way this is done for AGN is by reverberation mapping techniques (e.g., Kaspi et al. 2000). For all objects in our sample but one, reverberation masses were taken from Peterson et al. (2004). For one object in our sample (MCG-6-30-15) the mass was estimated from variability considerations and from the mass-velocity dispersion relation (McHardy et al. 2005).

Figure 1 shows the silicon band in the HETG spectra for all objects in our sample. Line signatures from highly ionized gas (specifically that of the Si XIV line near $\lambda 6.128$) are easily detectable. Thus, highly ionized absorbing gas is evidently present in *all* objects. This is an important finding since the sample was not pre-selected to detect such gas but rather to observe gas at much lower ionization levels pertaining to the so called “warm absorbing” phenomenon (e.g., George et al. 1998) and colder, more neutral, soft X-ray absorber. Gas at such high ionization levels would have evaded detection by previous observatories such as ASCA, but is clearly seen here. Moreover, the presence of this extremely ionized gas component in all objects reveals the existence of an important constituent of AGN. Indeed, the presence of such highly ionized gas in cases where outflowing warm absorbers are detected is

TABLE 1
 THE SAMPLE

Object	z	M_{BH}^* $10^6 M_{\odot}$	λL_{λ}^* erg s^{-1}	L_x erg s^{-1}	Γ_{ASCA}	α_{ox}	HETG time ksec
NGC 3783	0.00973	30 ± 5	43.26	43.4	1.8	1.1	680 (ObsID 2090, 2091, 2092, & 2094)
NGC 5548	0.01717	67 ± 3	43.51	43.8	1.9	1.05	150 (ObsID 3046)
NGC 7469	0.01632	12 ± 1	43.72	43.7	2.02	1.05	150 (ObsID 2956 & 3147)
NGC 4151	0.00332	13 ± 5	42.88	43.0	1.39	1.2	250 (ObsID 3052 & 3480)
MCG-6-30-15	0.00775	$4.5 \pm 3^{\dagger}$	42.4	43.1	2.1	0.8	500 (ObsID 4759, 4760, 4761, & 4762)
Total HETG time							~ 1700

* Taken from Peterson et al. (2004); Redshifts taken from Peterson et al. these differ from other values given in the literature by no more than 120 km/s

[†] Estimated from variability and the black-hole–bulge relation in galaxies; see McHardy et al. 2005

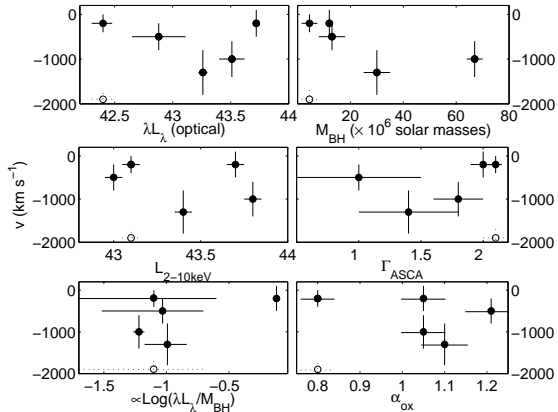


FIG. 2.— The outflow velocity as inferred from the Si XIV $\lambda 6.128$ absorption line for all objects in our sample as a function of object’s properties. Given the few number of points and the measurement uncertainties, no significant correlations can be seen in our sample. Nevertheless, it is clear that there is a wide range of outflow velocities for a given Eddington ratio. Uncertainties in the measured line velocity include wavelength position uncertainties as well as the effect of non-Gaussian line profiles (see text). It should be noted that redshifts toward individual may be uncertain by about 100 km s^{-1} (see Crenshaw et al. 1999).

naturally explained by the thermal wind picture of CN05. It is nevertheless unclear whether gas with even higher ionization levels is also outflowing in those objects (see e.g., Reeves et al. 2004) as the effective area and resolution of *Chandra* gratings is insufficient at the high energy band and the analysis of CCD spectra is of much lower resolution and is plagued with uncertainties related to photon redistribution effects.

The advantage of X-ray grating over non-grating spectra is that it allows us to unambiguously identify spectral features and measure absorption line velocities to great accuracy. We have measured the velocities of various silicon lines for all the objects in our sample and looked for correlations with other AGN properties; these are shown in figure 2. Clearly, no firm conclusions can be drawn from the small sample at hand. Nevertheless, it is indicative that the outflow velocity (as inferred from the Si XIV $\lambda 6.128$) is not intimately related to the Eddington ratio of the source and that AGN with apparently similar Eddington ratios can have HIG traveling with a wide range of velocities. The data hints at a possible trend between the flow velocity and the black hole mass. We caution however that this is dubious given the uncertainties involved and the small number statistics (note also that the appearance of a high velocity component in MCG-6-30-15 which does not agree with this trend and is further discussed in §4.4). No clear trends are seen as a function of the optical to X-ray luminosity slope, α_{ox} , the X-ray luminosity, the X-ray photon index, Γ_{ASCA} (George et al. 1998), or the optical luminosity, λL_{λ} (taken from Peterson et al. 2004 and for MCG-6-30-15

from George et al. 1998 using a typical type-I UV to optical conversion factor). Similar results are obtained for the outflow velocities inferred from other, non-blended, lines in the *Chandra*/HETG bandpass. In short, no clue as to the physical mechanism driving such flows in AGN may be drawn from the small sample at hand. The dependence of the other flow properties such as the column density, total opacity, ionization level, and temperature, is very model dependent and is not discussed here (see Blustin et al. 2005).

3. THE MODEL

Here we outline the model used in this work to derive the physical properties of the outflowing gas. This is based on a model extensively described in CN05 and applied to the outflowing gas in NGC 3783. Thus, we mention here only briefly the basic model ingredients and refer the reader to CN05 for an elaborate discussion and justification of the formalism.

The model used here is that for a multiphase, radiation and thermal pressure driven flow. The flow spans a range of densities at every location r (perhaps due to thermal instabilities or the onset of turbulence; CN05) and is assumed to obey a density-scale distribution of the form

$$\rho \propto \xi^{\beta} \quad (1)$$

where β is the powerlaw index (assumed constant throughout the flow and its value is to be determined from observations) and ξ is a measure of length. The ionization and thermal properties of each phase in the flow are self-consistently calculated using the photoionization code ION (e.g., Netzer 1996) which includes all relevant heating and cooling mechanisms. Self-shielding is self-consistently accounted for by our calculation scheme and we use the escape probability method to calculate emission line transfer either in static or differentially expanding media (see below). Once the ionization structure of the absorbing gas is obtained, the radiation pressure acceleration, a_{rad} is calculated taking into account all absorption and scattering processes such as bound-bound, bound-free, free-free absorption, as well as Compton scattering (see Chelouche & Netzer 2003). Complete knowledge of the gas thermal and ionization properties allows us to go one step further beyond pure photoionization models and consider the kinematic part of the problem at hand.

We first define the continuity condition for the outflowing gas. As shown in CN05, for a flow with a fixed density contrast ratio at all locations, the continuity condition for the most dilute component, i.e., that with the highest ionization parameter; $U_{\text{ox}}^{\text{max}}$ and lowest mass density, $\rho_{\text{min}}(r)$, is similar to the spherical expansion case and

$$\rho_{\text{min}}(r) \propto r^{-2} v(r)^{-1}. \quad (2)$$

The flow velocity, $v(r)$, is obtained by solving the general equation of motion for the multi-phase wind (assuming all phases are dynamically coupled) which takes the form,

$$\frac{1}{v} \frac{dv}{dr} = \frac{1}{v^2 - (1 + \beta/3)\gamma v_s^2} \left[\frac{2(1 + \beta/3)\gamma v_s^2}{r} - \frac{GM_{\text{BH}}^{\text{eff}}}{r^2} \right], \quad (3)$$

where v_s the sound speed at the critical point, r_c (see below) and γ the polytropic index (i.e., the gas temperature, $T \propto \rho^{\gamma-1}$). We note that γ is merely a parametrization which enables a relatively straightforward integration of the equation of motion and whose value depends, as far as the dynamical problem is concerned, on the heating and cooling processes of the most ionized flow phase; e.g., photo-heating, radiative cooling, adiabatic expansion, and possibly other heating mechanisms such as dissipation of turbulent energy (e.g., CN05). $\gamma = 1$ corresponds to isothermal gas. We define the effective black hole mass, $M_{\text{BH}}^{\text{eff}}$ as

$$M_{\text{BH}}^{\text{eff}} \equiv M_{\text{BH}} \left(1 - \frac{\langle a_{\text{rad}} \rangle}{g} \right) \quad (4)$$

where g is the gravity (for a non- or a highly sub-Keplerian rotating flow, $M_{\text{BH}}^{\text{eff}}$ has only a very weak dependence on r ; CN05), and $\langle a_{\text{rad}} \rangle$ is the average radiation pressure acceleration at a given location in the flow defined as

$$\langle a_{\text{rad}}(r) \rangle = \frac{\int dm a_{\text{rad}}(\rho; r)}{\int dm}, \quad (5)$$

where $dm = \rho dV(\rho)$ is the contribution to the mass from each flow phase. As $\langle a_{\text{rad}} \rangle$ depends on the local properties of the flow such as the ionization, temperature, density contrast, it is not known a-priori and must be solved in conjunction with the equation of motion. Figure 3 shows $\langle a_{\text{rad}} \rangle / g$ for a source emitting at its Eddington rate ($g = g_{\text{Edd}}$). Clearly, for all plausible values of β and $U_{\text{ox}}^{\text{max}}$, the radiation pressure acceleration barely exceeds that due to Compton radiation pressure (i.e., unity in the adopted units). This property allows this term to be neglected in the CN05 analysis of NGC 3783 due to the low Eddington rate of the source ($g \gg g_{\text{Edd}}$ hence $\langle a_{\text{rad}} \rangle / g \ll 1$). Nevertheless, the radiation pressure acceleration can have a non-negligible effect on the dynamics for sources emitting close to their Eddington rate (such may be the case of NGC 7469 in our sample).

The equation of motion requires that a steady-state solution be initially subsonic and reach super-sonic velocities while passing through a critical point where both the numerator and the denominator vanish (e.g., Parker 1965). This point is given by

$$r_c = [(1 + \beta/3)\gamma]^{-1} \frac{GM_{\text{BH}}^{\text{eff}}}{2v_s^2}, \quad v(r_c) = v_s \sqrt{(1 + \beta/3)\gamma}. \quad (6)$$

Once the flow density and velocity are determined by the model at some location along flow lines and assuming a divergence free flow (i.e., there are no mass sinks or sources) the mass loss rate is given by (CN05),

$$\dot{M} = C_{\text{global}} \frac{8\pi r^2 \rho_{\text{min}} v}{\beta + 2} \frac{1 - (\rho_{\text{max}}/\rho_{\text{min}})^{(\beta+2)/\beta}}{1 - (\rho_{\text{max}}/\rho_{\text{min}})^{2/\beta}}. \quad (7)$$

where C_{global} is the global (in units of 4π) covering factor.

The equation of motion (eq. 3) combined with the continuity condition (eq. 2) must be solved in conjunction with

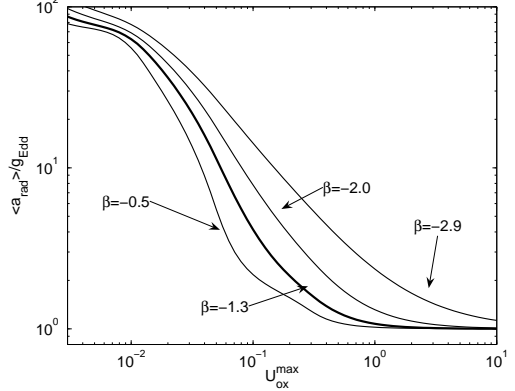


FIG. 3.— The average radiation pressure acceleration relative to gravity (for a source emitting at its Eddington rate) as a function of the maximum ionization parameter in the flow, $U_{\text{ox}}^{\text{max}}$ and for several values of the density spectrum powerlaw index β . The minimum ionization parameter, $U_{\text{ox}}^{\text{min}}$ in the flow was arbitrarily set to 10^{-4} and its exact value has little effect on the results. Clearly, the mean radiation pressure acceleration is not much larger than the Compton pressure for plausible values of the parameters (see e.g., CN05, and table 2). This implies that radiation pressure force on the HIG kinematics may be neglected in objects emitting below their Eddington rate.

the photoionization and thermal equations to yield a self-consistent solution for the structure and dynamics of the outflowing gas. We note that self-shielding can be important and is accounted for by our model. The model also includes the effects of adiabatic cooling as well as a possible additional heating source in the form of dissipation of turbulent energy. We refer the reader to CN05 for the detailed layout of the model and our calculation scheme. Throughout this work we assume solar composition gas (see Arav et al. 2001, 2007, Netzer et al. 2003 and references therein). Once the velocity profile and the flow ionization and thermal structure are known for every phase at every location, we calculate the transmitted spectrum through the flow including all important lines and edges while accounting for the differential expansion of the flow via the CN05 formalism. The synthetic spectrum is then convolved with the instrumental kernel (assumed Gaussian) and is compared to the data.

A comparison of the model prediction to the observed line profiles as well as to the continuum shape allows us to constrain the parameters of the model which include the location at which the flow crosses our line of sight, r_0 (this needs not be equal to r_c as lines can be detached; see e.g., Arav 1996 and CN05), the range of ionization parameters occupied by the flow at r_0 , $[U_{\text{ox}}^{\text{min}}, U_{\text{ox}}^{\text{max}}]$, and β . Once these parameters are set the entire solution is determined, hence the absorption spectrum. We note that in addition to the above parameters that characterize the outflow, the object's luminosity, black hole mass, and its intrinsic spectral energy distribution must also be specified.

Our fitting procedure is fully interactive due to the complexity of the model. We first look for the highest ionization species identifiable in the absorption spectrum. These allow us to estimate or put a lower bound on $U_{\text{ox}}^{\text{max}}$. This is important since the highest ionization component sets the dynamics of the entire multi-phase flow (CN05). From the low ionization silicon lines (and to some extent also the continuum shape at soft X-rays; but see §4.3, 4.4), we can estimate $U_{\text{ox}}^{\text{min}}$ and set the density contrast ratio in the flow. Estimating $U_{\text{ox}}^{\text{min}}$ from observations is more challenging than deducing the value of $U_{\text{ox}}^{\text{max}}$ due to uncertainties in the shape of the soft X-ray con-

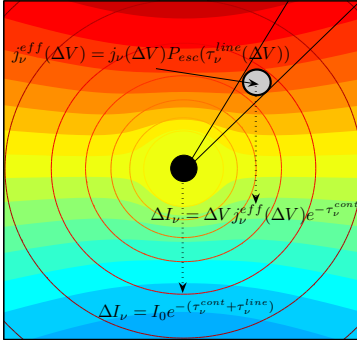


FIG. 4.— Schematics of the iso-velocity contours of a wind model as seen by an observer at the bottom of the diagram. Also shown is a parcel of the outflowing gas which emits line photons. Within the parcel we assume the effective line emissivity, j_ν^{eff} to be the product of the intrinsic emissivity, j_ν and the static escape probability, P_{esc} (assuming the static case applies; see text). Continuum attenuation is then calculated along the photon path from its creation point to the observer.

tinuum, yet this has a negligible effect on the derived mass loss rates and the kinetics luminosities. The powerlaw index β can be constrained by its combined effect on the spectral shape and on the gas dynamics (CN05).

Once an acceptable fit is found (given the criteria used in CN05), the physical properties of the outflowing gas and the uncertainties on individual parameters are obtained by manually changing their values and then searching for an adequate agreement between the model and the data by varying all other parameters of the model (e.g., β , r_c , r_0 , C_{global} , $U_{\text{ox}}^{\text{max}}$, and the density contrast). Thus, the quoted errors are not independent among different parameters and inter-correlations exist between them (see CN05 for further details).

3.1. Emission line treatment

Once an adequate model is found based on a global agreement with the absorption data and the flow structure and dynamics are constrained, we calculate the emission spectrum from the outflowing gas. For this purpose we assume that the global flow structure for all lines of sight is similar to the one which is intercepted by us. While this may not be true in general (e.g., Kaspi et al. 2004), it is the only viable approach to the problem at this stage. Calculating the emission spectrum from a differentially expanding medium is an extremely complicated task and requires detailed ray-tracing calculations for hundreds of lines. Here we take a very simplified approach which, despite its limitations (see below), accounts in a better way for the emission lines from such flows.

Previous works (e.g., Netzer et al. 2003) have calculated the emission spectrum assuming stationary gas. Nevertheless, photon scattering in differentially expanding medium is limited to sections of the flow having similar velocities up to roughly one "thermal" width (by "thermal" we mean either purely thermal or that which is set by small scale turbulent velocity field, so called micro-turbulence). For larger velocity differences, the absorption cross-section is considerably reduced and photon scattering is less important. This is the basic notion behind the well established Sobolev approximation which we use here for treating emission lines. We therefore divide the flow into segments in 3D space such that they are independent of one another with respect to photon scattering in lines. We assume that different transitions do not overlap

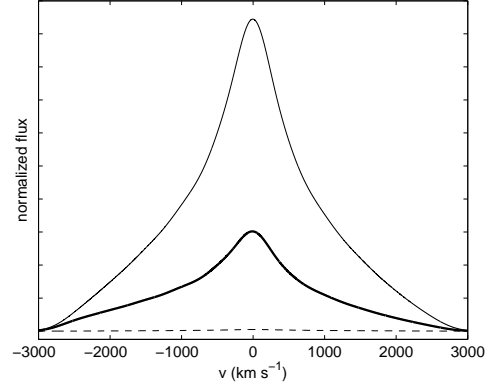


FIG. 5.— The emission line profiles from a spherically symmetric expanding flow when calculated using the full scheme described in text (thin line) and compared to the case in which no continuum absorption of line photons is assumed (thick line). Clearly, the difference between the two methods is considerable and detailed calculations are necessary to constrain the global covering factor of the flow. We also note the asymmetry of the fully calculated line profile due to stronger absorption of the receding part of the flow.

in energy space which is good enough an approximation for the relatively low velocities considered here (e.g., Chelouche & Netzer 2003; see however the O VI λ 21.87 line problem, Netzer et al. 2003). Naturally, different lines have different thermal widths, and this is further complicated by the possible emergence of turbulence (e.g., CN05). We take the simplified approach in which all lines are affected similarly and use the gas sound speed of the highest ionization component as a measure of the line width for all lines. Within each flow segment we calculate the emergent spectrum assuming it to be stationary in its own frame (i.e., we neglect differential expansion within individual segments). We use the static approach (e.g., Netzer 1996 and references therein) in the subsonic part of the wind. While this treatment of the emission line transfer is approximate even within the framework of the escape probability method, the uncertainties associated with the unknown global geometry of the outflowing gas are likely to dominate (e.g., Bonilha et al. 1979). The emission spectrum is calculated by summing over the contribution from all flow segments and accounting for the velocity shifts between them. A major concern using this scheme is the effect of continuum absorption on the line flux (see figure 4). Contrary to lines, this process is non-resonant; i.e., photons do not scatter but are absorbed by gas lying in our line-of-sight to the point of creation of the photon. While for most cases in our sample this effect causes line fluxes to differ by roughly 20% (this was verified by calculating the emission spectra assuming complete absorption by the flow and no absorption at all), for one object in our sample (NGC 4151) the effect turns out to be substantial.

The wavelength dependent continuum optical depth for a photon created at some location r' , θ' within the flow is

$$\tau_\nu^{\text{cont}}(r', \theta') = \left[-\text{sign}(\cos\theta') \int_{r'}^{r' \sin\theta'} + \int_{r' \sin\theta'}^{\infty} \right] \times \left(\frac{d\tau_\nu^{\text{cont}}}{dr} \right) \sqrt{1 - \frac{r'^2}{r^2} \sin^2\theta' dr} \quad (8)$$

Once the flow opacity profile is constrained by our model for a single line of sight, and assuming spherical symmetry, the above integral can be readily calculated numerically at every frequency, and the process can be repeated for all emission

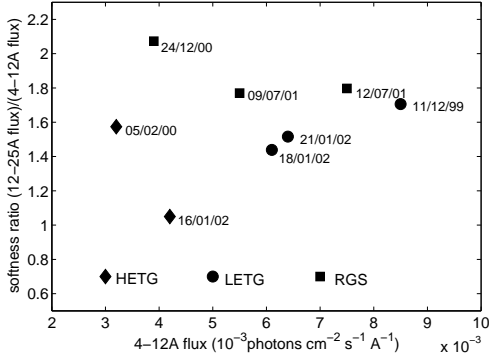


FIG. 6.— The softness ratio as a function of the hard X-ray flux for eight X-ray grating observations of NGC 5548 (three *Chandra/LETG*, two *Chandra/HETG*, and two *XMM/RGS*). Clearly, there is no correlation between the softness ratio and the flux level. This is similar to the behavior of NGC 3783 which was reported by Netzer et al. (2003).

lines. Depending on the number of zones required (i.e., on the sound-speed of the gas), the calculation may take several hours on a Linux workstation (we note that, for the specific case in which $d\tau/dr$ is a powerlaw of r , a semi-analytic form for the integral exists employing the Hypergeometric functions). Figure 5 demonstrates the different emission line fluxes and profiles obtained by assuming no/full continuum absorption of the emitting region, and accounting for the flow geometry in full as described above. The line intensity is different as well as the line profile being slightly asymmetric in the full calculation due to higher flow opacity toward the receding side compared to the approaching side. The full radiative transfer yields emission lines with intermediate intensities due to geometry affecting the extended emission region.

When calculating the integrated emission spectrum we include the contribution of all phases of the flow at every location and the emission/absorption spectra are combined. We note that due to the unknown geometry of the emission region with respect to our viewing angle, spherical symmetry is assumed. By changing the global covering factor of the emitting gas, C_{global} , we do not alter the geometry of the flow but rather rescale its overall contribution to the flux. Again, this approach is probably a crude over-simplification yet we believe it is the only viable assumption at this stage. The resulting emission/absorption spectrum depends on the parameters of the model and a comparison with the spectral data may be used to deduce their values.

4. RESULTS

In this section we discuss our results pertaining to the spectra of individual objects in our sample. The detailed analysis for each object is presented separately since, despite their overall similarities, their properties and their spectra can differ substantially. The implications of our results are discussed in section 5.

4.1. NGC 5548

NGC 5548 is a typical type-I Seyfert galaxy and has perhaps the best studied warm absorbing gas after NGC 3783 (Kaastra et al. 2000). The hard X-ray (1–10 keV) photon slope is known to vary in the range 1.5–1.7 (Chiang & Blaes 2003) with a mean value of 1.6 (Kaastra et al. 2004). There is evidence for a steep soft X-ray slope (Kaastra et al. 2004) reminiscent of the case of NGC 3783 (Netzer et al. 2003). The

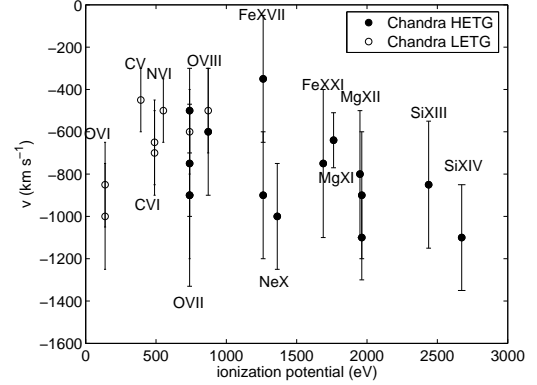


FIG. 7.— Line velocity as measured from *Chandra* HETG and LETG observations of NGC 5548. Our measurements do not show a significant correlation between the velocity of the line transition(s) and the ionization potential of the ion giving rise to those transitions. This is similar to the case of NGC 3783 (see however Steenbrugge et al. 2005 and text).

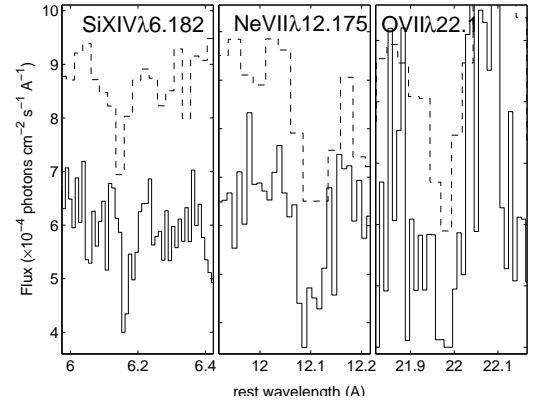


FIG. 8.— A comparison between the HETG (solid line) and LETG (dashed line) data for NGC 5548 which were taken at different epochs. There is an evident shift of high ionization lines to higher velocities compared to low ionization lines in the LETG data. This may be either due to changes in the flow opacity at high ionization levels during the LETG epoch or due to wavelength calibration issues between the instruments (see also Steenbrugge et al. 2005).

optical to X-ray spectral slope, α_{ox} is also similar to that of NGC 3783 (see table 1). Thus, there is no direct evidence that the ionizing spectra of NGC 5548 and NGC 3783 differ substantially and, for the purpose of our model, we assume they are identical and, therefore, use the ionizing continuum shape defined in Netzer et al. (2003). We find the bolometric luminosity of the NGC 5548 (given its mean 2–10 keV X-ray flux reported by Steenbrugge et al. 2003) to be $\sim 7 \times 10^{44}$ erg s^{-1} and conclude that the Eddington ratio is ~ 0.1 , i.e., comparable to that of NGC 3783.

NGC 5548 has been observed three times by *XMM* (e.g., Steenbrugge et al. 2003, Pounds et al. 2003) and five times by *Chandra* (two *HETG* and three *LETG* observations; e.g., Kaastra et al. 2002). The object was found to vary by nearly a factor four in luminosity over a period of three years. The spectral shape (expressed here by the softness ratio; see figure 6) also varied by $\sim 40\%$ during that period with no obvious correlation with the flux level (see also Kaastra et al. 2004). This behaviour is very similar to the one reported by Netzer et al. (2003) for NGC 3783 and suggests a common physical mechanism that drives these phenomena in both objects. From spectral analysis of X-ray absorption fea-

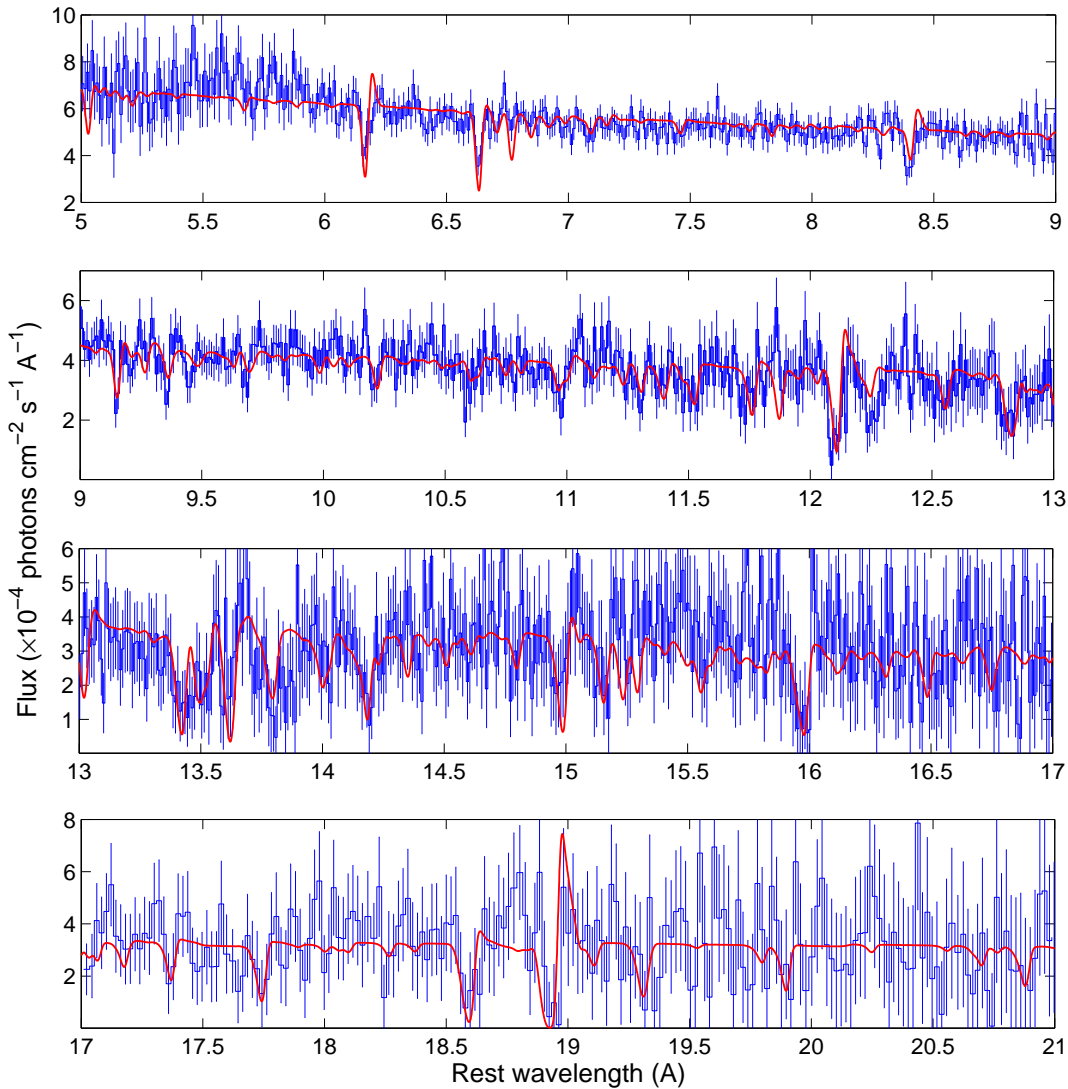


FIG. 9.— A spectral model for a thermally driven wind overlaid on the *Chandra*/HETG spectra of NGC 5548. Clearly, the model reproduces most absorption line features and traces well the continuum shape over almost a decade in photon frequency. Some residuals near 15Å are possibly due to uncertainties in the di-electronic recombination coefficients of iron (e.g., Netzer 2004). Contribution of the outflow to the emission is clearly evident. Note that data binning is different between the panels.

tures, Steenbrugge et al. (2003, 2005) conclude that the HIG is highly stratified and spans a large range of temperatures ($\sim 10^4 - 10^6$ K). A similar conclusion was reached by Netzer et al. (2003) and CN05 for the X-ray outflow in NGC 3783. Detailed photoionization modelling of the HIG in both objects suggest that low ionization gas components have smaller column densities than the high ionization ones (with a qualitatively similar scale dependence obtained for both objects; c.f. Steenbrugge et al. 2005 and CN05). The outflow velocity in both objects is also similar as has been verified by observations of several absorption lines (cf. Kaspi et al. 2002 and Steenbrugge et al. 2005). Neither the HIG in NGC 5548, nor that in NGC 3783 show clear response with respect to variations of the continuum flux level of the source implying, by recombination time-scale arguments, that the flow is located on parsec scales.

We have measured the line velocities for the high ionization

species from the *Chandra* HETG and LETG observations (see figure 7). For high ionization lines we rely on measurements from the HETG which has a higher spectral resolution. We find no clear trend between the ionization level (expressed here using the photoionization threshold energy of the ion) and the velocity. We compared the LETG and HETG spectrum (see figure 8) and find that high ionization LETG lines are more blueshifted compared to the HETG lines. The cause for this may be either due to changes in the flow opacity with time which are manifested only in relatively high ionization lines (e.g., Si XIV λ 6.182 and Si XI λ 6.778), or calibration issues. While the underlying reason for the discrepancy is unclear, this is probably the cause for the different result in our work compared to Steenbrugge et al. (2005).

Motivated by the above similarities between NGC 5548 and NGC 3783 we attempted to explain the highly ionized outflow in NGC 5548 with a model similar to the one presented

in CN05. Our fitting procedure follows the scheme presented in §3 and discussed in CN05. Here too, we find the effect of radiation pressure acceleration on the flow dynamics to be negligible (i.e., $\langle a_{\text{rad}} \rangle / g \ll 1$; see figure 3). The best-fit underlying photon powerlaw index is 1.6 (i.e., similar to that of NGC 3783) and our scheme converges to an acceptable spectral model shown in figure 9 and whose parameters are given in table 2. We have tried models with and without additional heating sources, like in the case of NGC 3783. We arrive to the same conclusions as in CN05 regarding the necessity for an additional heating source, perhaps due to the dissipation of turbulence to counter-balance the effect of adiabatic cooling. Excluding an additional input of heat will result in a similar overall fit to the continuum shape only with narrower and less blueshifted lines which are less favored by the data (see also CN05).

Clearly, the model traces well the continuum and lines of the more abundant elements but over-estimates the absorption due to Si XIII and Si XIV at around 6.5\AA . There are several possible reasons for that: the first is that the abundance of silicon is somewhat lower than solar. Our calculations show that the data are consistent with the abundance of silicon being roughly 30% solar. Evidence for deviations from solar composition have been previously suggested to explain the UV absorption line spectrum of quasar outflows (e.g., Arav et al. 2001, 2007). Troughs may appear deeper in our model due to under-estimated emission whose normalization is derived from global fitting. It is also possible that the over-estimation of the absorption by highly ionized silicon lines is related to time-dependent ionization. For the densities implied by our model ($\sim 10^3 - 10^6 \text{ cm}^{-3}$ at r_0), we find that the equilibration timescales are of order a week (Krolik & Kriss 2000; correcting for the different density and flux). Hence, the ionization level depends on the long-term history of the flux and SED of the source. Unfortunately, we do not have such data at hand. Nevertheless, there is a clear indication that the object brightened in the hard band by about 50% over a period of 2 days (see figure 6) and is expected to result in some deviation from a pure ionization equilibrium case. These would be again small if the equilibration timescale is much longer than the variation timescale; indeed comparing the LETG observation taken two days prior to the first HETG observation shows no significant changes in the lines apart from what we suspect to be due to calibration effects. Last is the possibility of thermal instability driving some of the gas to higher temperatures so that more of the gas becomes transparent and not contribute to the silicon line opacity. The time-dependence of thermal instability phenomenon has not been studied in detail for such gas and its proper treatment is beyond the scope of this paper.

In addition to the above discrepancy, our model is slightly below the data around 15.5\AA . This problem was already noted by CN05 and likely results from uncertainties in the dielectronic recombination rates of iron (e.g., Netzer 2003) as well as uncertainties in the properties of the unresolved transition array (UTA) of iron whose most up-to-date values (Gu et al. 2006) have not been incorporated into our calculation scheme.

The calculation of the mass loss rate requires knowledge of the global covering fraction of the absorber, C_{global} . This can be obtained by fitting for the emission lines. This is accomplished here by assuming that the flux level of the source represents its long-term average and that it has not varied signif-

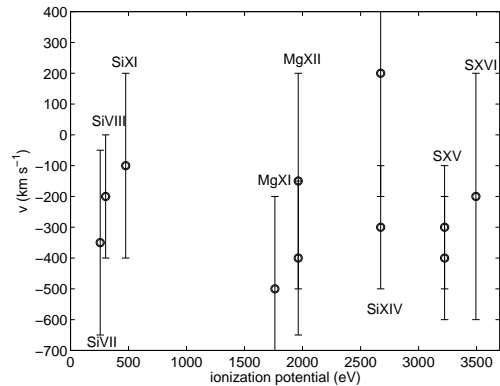


FIG. 10.— Line velocity as measured from *Chandra* HETG observations of NGC 4151. Here too, our measurements show no clear correlation of the velocity with ionization potential.

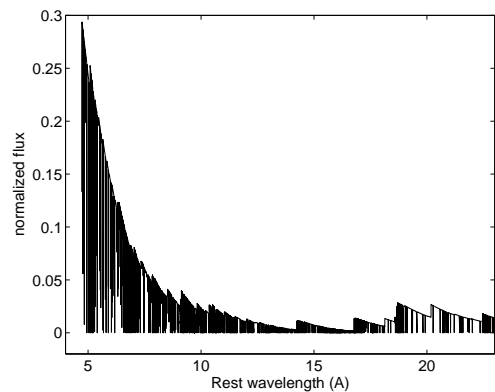


FIG. 11.— The best-fit model for the transmitted spectra through the outflowing for NGC 4151 shows considerable opacity at long wavelengths. Clearly, absorption is also important even at short wavelengths (cf. Kraemer et al. 2005). Accounting for the absorption we obtain a canonical photon powerlaw index, $\Gamma_{\text{ph}} = 1.6$ (see text).

icantly over the equilibration timescale of the ionized gas and the light crossing time of the emission region (as discussed above this assumption may not be well justified yet it is the only viable one at this stage). Our model suggests that the data are consistent with the flow fully covering the ionizing source and is therefore different from the case of NGC 3783 (Netzer et al. 2003). This is expected given the similar equivalent width of the emission lines for the two objects (e.g., oxygen lines, compare Kaspi et al. 2003 and Steenbrugge et al. 2005) while noting that the column density of the absorber in NGC 5548 is smaller by a factor of a few. The obtained mass loss rate and the kinetic luminosity associated with the flow are given in table 2.

4.2. NGC 4151

NGC 4151 is classified as a Seyfert 1.5. Its UV spectrum is characterized by multi-component absorption systems with a range of outflow velocities ($0-1600 \text{ km s}^{-1}$) and with derived absorber distances in the range $0.03-2100 \text{ pc}$ (Kraemer et al. 2001). The object is known to be highly variable in the X-rays (cf. Perola et al. 1982, 1986) showing a complex spectral behavior indicating possible transverse motion of the X-ray absorber and/or ionization changes triggered by flux variation (e.g., George et al. 1998). Ogle et al. (2000) have resolved extended emission on kpc scales which motivated Schurch et

TABLE 2
 BEST-FIT MODEL PARAMETERS

Parameter	NGC 3783	NGC 5548	NGC 7469 ^(a)	NGC 4151	MCG-6-30-15 (low/high)
Critical distance r_c [10^{18} cm]	2.0 ± 1.5	7 ± 2	1.0 ± 0.5	1.5 ± 0.8	$(8 \pm 8 / 0.2 \pm 0.15)$
Line-of-sight crossing distance r_0 [10^{18} cm]	5 ± 2	6 ± 2	1.0 ± 0.5	0.3 ± 0.2	$(10 \pm 7 / 2 \pm 1)$
Maximum ionization parameter at r_0 [$\log(U_{\text{ox}}^{\text{max}})$]	0.5 ± 0.3	0.1 ± 0.3	0.7 ± 0.7	-0.3 ± 0.5	$(-0.2 \pm 0.5 / 0.5 \pm 0.3)$
Minimum ionization parameter at r_0 [$\log(U_{\text{ox}}^{\text{min}})$]	-3.7 ± 1.5	-4 ± 1	-3.0 ± 1.5	-4 ± 1	$(-2.5 \pm 1.0 / -3 \pm 1)$
Density spectrum index (β)	-1.2 ± 0.5	-1.4 ± 0.6	-1.3 ± 0.6	-1.4 ± 0.3	$(-1.3 \pm 0.6 / -1.3 \pm 0.5)$
Global covering factor ^(b) , C_{global}	0.2	1	1	1	$(0.7 / 1.0)$
Mass loss rate [$\log(M_{\odot} \text{ yr}^{-1})$],	-1.5 ± 0.5	-0.2 ± 0.6	-2.0 ± 0.8	-3.2 ± 0.7	$(-1.0 \pm 0.8 / -2.2 \pm 0.7)$
Mass accretion rate ($= 90\lambda L_{\lambda}/c^2$) [$\log(M_{\odot} \text{ yr}^{-1})$]	-1.7	-1.5	-1.3	-2.2	-2.6
Relative Kinetic Luminosity (L_{kin}/L) ^(c) [per cent]	0.01	0.1	0.0001	0.0001	0.02

^(a) The effective mass of NGC 7469 has a large uncertainty. The quoted errors assume the object emits at about 90% of its Eddington rate. While the object could, in principal, emit more efficiently, we find it less likely for reasons described in text

^(b) We note that the global covering fraction was derived assuming spherical symmetry for the absorbing gas and assuming that the outflowing matter is solely responsible to the emission. If other components are responsible for the emission then C_{global} reported here is only an upper limit. The covering factor for NGC 3783 was taken from Netzer et al. (2003)

^(c) The bolometric luminosity, $L \simeq 9 \times \lambda L_{\lambda}$ (e.g., Kaspi et al. 2000 and references therein) and the kinetic luminosity was calculated in two ways: taking the velocity of the Si XIV $\lambda 6.148$ line, and taking the highest velocity measured for any line (for a specific flow component in MCG-6-30-15).

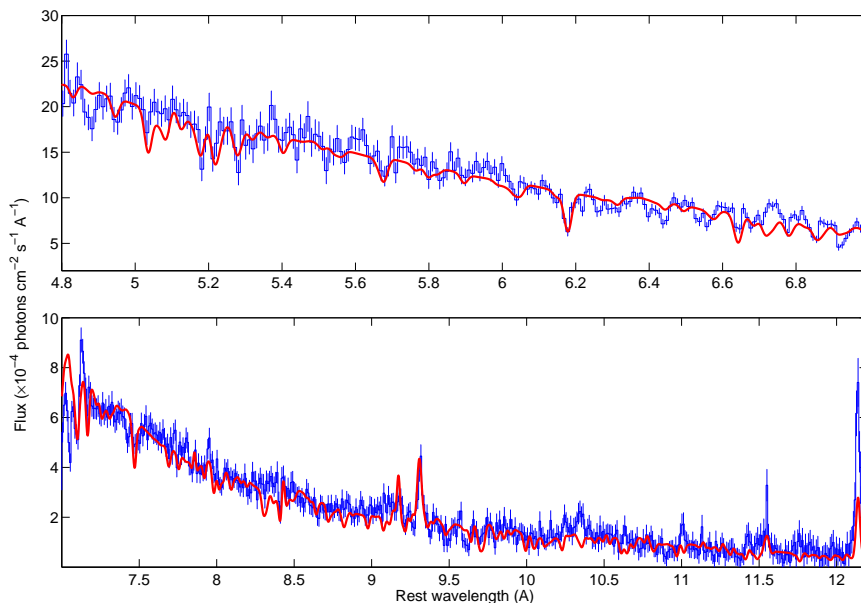


FIG. 12.— An outflow model overlaid on the *Chandra*/HETG spectra of NGC 4151 (corrected for galactic absorption with a column $2.2 \times 10^{20} \text{ cm}^{-2}$; George et al. 1998). Clearly, the fit is able to reproduce many spectral features including absorption lines and the shape of the ionizing continuum. That said, the model fails to account for all features in the spectrum and under-estimates the strength of some emission lines (see text).

al (2004) to apply an ionization cone model while trying to establish an X-ray unification scheme for AGN. The HETG spectra (see also Kraemer et al. 2005) is emission dominated for wavelengths greater than $\sim 9 \text{ \AA}$ and the continuum is hard. Luckily, the silicon absorption line band at short wavelengths has good S/N which allows a detailed investigation of the HIG flow. We have analyzed all the HETG observations for this object. In the two more recent observations (ObsID 3052 & ObsID 3480) the X-ray flux and the spectral shape were very similar while in a previous one (ObsID 335), the hard X-ray continuum level was lower and the spectral shape different. Thus, we concentrate here on the two recent HETG observations and analyze their combined spectra resulting in high S/N data. Inspection of individual lines reveals that there is no significant correlation between velocity and ionization level (fig-

ure 10). Also, the high velocity ($\gtrsim 1000 \text{ km s}^{-1}$) UV components (component A and B in Kraemer et al. 2001) may have little X-ray opacity and are not clearly detected here.

Our objective here is to find the simplest model possible (i.e., with the least number of free parameters) which would explain the global spectral shape of the source as well as individual line profiles. Thus, we attempted to apply a single outflow model to the data *assuming* that the underlying continuum shape is similar to that of NGC 3783 and NGC 5548 and that the current continuum level represents the long term (compared to equilibration and light crossing timescales) average of the source. We find that it is possible to meet many of the observational constraints by a single flow model whose spectral features are shown in figure 11. Clearly, the model is very optically thick with considerable absorption

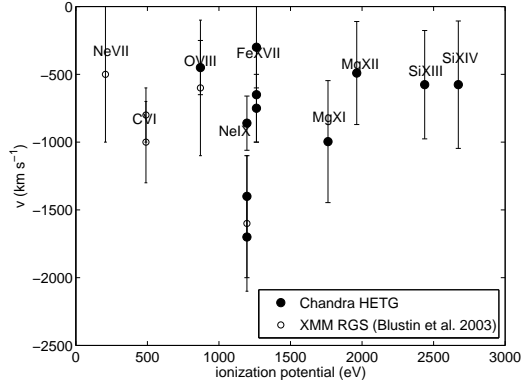


FIG. 13.— Line velocity vs. the ionization potential of the ion responsible for the transition as measured from *Chandra* spectrum of NGC 7469. The data are augmented by the measurements by Blustin et al. (2003) from XMM-RGS observation of the object. Clearly, there is no clear trend between the ionization potential and the line velocity; a behavior which is similar to that seen in other objects in our sample.

even at short wavelengths. The EW of the narrow iron line ($\sim 17.5 \pm 4 \text{ m\AA}$ according to our measurements) is typical of non-absorbed type-I AGN (cf. Kaspi et al. 2001) and is consistent with a scenario in which the absorber covers the iron $K\alpha$ line emitting region. As before, we have tried this model with and without additional heating source. Including such a source results in a slightly better fit to the lines.

A comparison between the data and the model is shown in figure 12. The overall agreement is satisfactory yet there are notable exceptions such as the under-prediction of some emission lines even for a flow fully covering the ionizing source. As noted previously by several authors (e.g., Ogle et al. 2001), NGC 4151 shows evidence for extended emission, thus it is not at all surprising that our model under-predicts some emission lines. Best fit model parameters are given in table 2. We note that the minimum ionization parameter at r_0 is lower by a factor of a few than that which characterizes the other objects in our sample. This is, however, consistent with the general picture whereby our line-of-sight through the wind penetrates deeper into parts of the outflow below the critical point. At such sections of the outflow, the densities are higher and the continuity condition results in the flow having somewhat lower ionization levels.

Attributing the changes in the X-ray spectrum over a period of two years to line-of-sight crossing of the absorber have led Kraemer et al. (2005) to conclude that a considerable amount of optically thick gas lies approximately 10^{17} cm from the ionizing source. This is in rough agreement with our distance estimate for the optically thick part of the flow (see table 2). Thus, if our model is correct then the prominent X-ray absorber is probably related to the $D+E$ UV components (Kraemer et al. 2005). A more detailed investigation of the UV–X-ray connection in this and other objects is beyond the scope of this paper.

4.3. NGC 7469

NGC 7469 is classified as a Seyfert 1.2 galaxy and its mean luminosity and black hole mass (as deduced from both reverberation and variability; see Nikolajuk et al. 2004) indicate that it is accreting near the Eddington rate (e.g., Petrucci et al. 2004). There is evidence for a complex behavior of the X-ray slope, or alternatively the hardness ratio, as a function of the hard X-ray flux which is reminiscent of what is ob-

served in NGC 3783 and NGC 5548 (see figure 3 in Nandra et al. 2000). Analysis of the high resolution X-ray grating spectrum taken for this object by *Chandra* shows no significant correlation between the ionization threshold of the ion and the corresponding velocity (figure 13).

In this case the contribution of radiation pressure force relative to gravity cannot be neglected since the Compton radiation pressure force is of the order of the gravitational force. This results in the effective black hole mass, hence the critical radius, being smaller. Nevertheless, below the critical point gravity must prevail for the flow to be stationary. This can happen if the gas near its footpoint is exposed to a different ionizing continuum and/or luminosity either by self-shielding, geometrical effects, or their combination. Another possibility is that the present continuum level is not representative of its long term (comparable to or larger than the dynamical timescale) average and that the flow was launched when the object was emitting at sub-Eddington rates. Currently, it is not known which of these scenarios is more realistic and we proceed under the assumption that the current flux level represents a long term average for this source.

Given the large uncertainty on the mass and the fact that radiation pressure force and gravity are of the same order of magnitude, the uncertainty in the effective gravity is very large. As the line troughs are not significantly detached the flow crosses our line-of-sight around its critical point. As there is no significant soft X-ray absorption, the flow is optically thin and therefore it is unlikely that gravity prevails at the sub-sonic part due to considerable opacity. Thus, we continue under the assumption that the object emits at sub- (although close to) the Eddington rate. As a starting point we assume it emits at $0.9L_{\text{Edd}}$ and check the sensitivity of the derived flow parameters to this assumption later on. The effect of adiabatic cooling is negligible due to the high Eddington rate (Begelman, McKee, & Shields 1983) and an additional heating source is not required by the data.

We have attempted to explain the continuum shape and lines using a single powerlaw for the underlying (unabsorbed) continuum extending from soft to hard X-ray energies. Our calculations show that a single powerlaw model fails to account for the spectral shape of both the soft and hard X-ray spectral bands and that the powerlaw steepens towards lower energies. (An alternative explanation of a single powerlaw with a photon slope, $\Gamma_{\text{ph}} \sim 2.3$ fails to account for the spectral shape near ~ 1 keV and over-predicts the strength of the absorption lines.) The presence of a soft excess is by no means surprising; in fact, it is expected to be more prominent in objects accreting near their Eddington rate (e.g., Wang & Netzer 2003, Matsumoto et al. 2004). Our model suggests that a good agreement between the model and the data is obtained if Γ_{ph} for the hard (> 1 keV) X-ray band is ~ 1.9 while at lower energies $\Gamma_{\text{ph}} \sim 3.5$ (the relative normalization of which is ~ 0.3 at 1 keV). The data quality is not good enough to tell whether partial covering effects are important in the soft X-rays since the lines are weak and the S/N low. As for the emission lines, these are weak and are likely to be absorbed by the outflowing gas given the low velocity dispersion of the flow. The data are consistent with an absorbing/emitting outflow that fully covers the ionizing source though we note that this is only an upper limit and that the true coverage can be much less than unity.

The outflow model is relatively optically thin at all wavebands and a comparison between the data and the model is shown in figure 14. The overall agreement is good with no

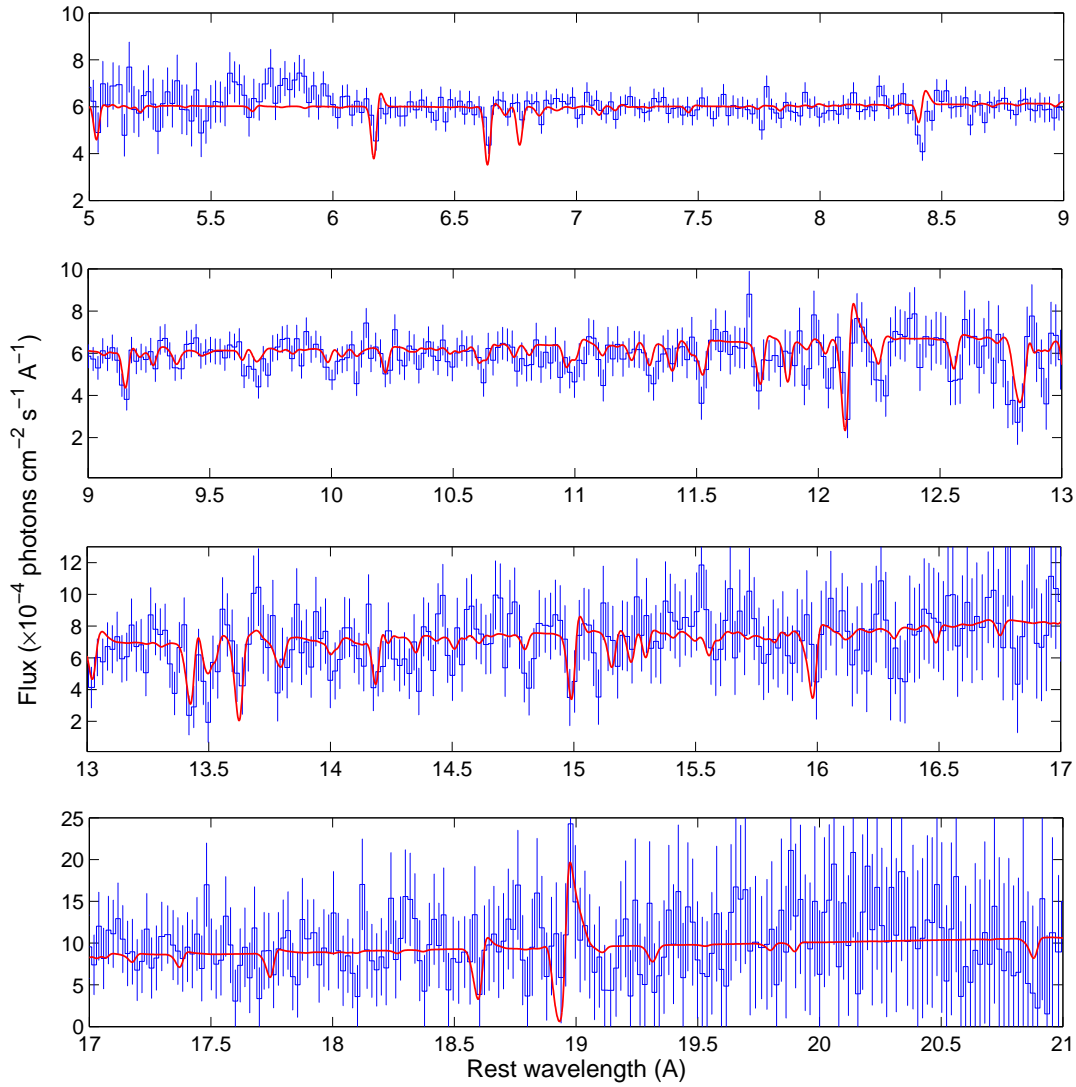


FIG. 14.— An outflow model to the *Chandra*/HETG spectra of NGC 7469. Clearly, the model reproduces most absorption features. Unlike other objects in our sample, NGC 7469 shows a soft excess requiring the use of different photon slopes at the short and long wavelength bands (see text). This is not unexpected given that this object is thought to radiate close to its Eddington rate and, as such, may be similar to narrow line Seyfert 1 galaxies.

apparent deviations apart from a calibration issue shortward of 6\AA at the interface between two chips.

The best-fit model parameters are shown in table 2. We note that our choice of effective black hole mass was somewhat arbitrary and that the source can emit even closer to its Eddington rate, say at 95% of its Eddington luminosity. In this case the effective gravity is smaller and the critical point moves closer in. Thus, our predicted location of the flow in this object is rather uncertain. This has some bearing on the other parameters of the model whose errors are somewhat larger than those for the other objects in our sample. These uncertainties can only be reduced by better measuring the black hole mass and determining the shape of the ionizing continuum, or by measuring ionization equilibration timescales for the plasma. It is interesting to note that, given the uncertainty on the effective gravitational term, the flow can, in principle, be launched just outside the broad line region (BLR) for this object (located at around 10^{16} cm; Kaspi et al. 2000). This,

however, requires somewhat different parameter values than those derived for flows in other objects. Specifically, for flows which are launched much closer to the inner engine, larger values of β are needed to maintain the same opacity as the flow is launched closer to the ionizing source. We find this explanation less likely since β is expected to be governed by the microphysics of the gas rather than the properties of the AGN. Thus, based on the similarity of flows in different objects we expect the flow in NGC 4151 to be launched at somewhat larger distances than the BLR.

4.4. MCG-6-30-15

MCG-6-30-15 is a borderline narrow Seyfert 1 galaxy that has been the center of an ongoing debate concerning the properties of its soft X-ray spectrum (see Sako et al. 2001). We wish to emphasize that here we do not attempt to resolve this debate which, in our opinion, requires a deeper understanding of the soft X-ray spectrum of AGN. While in the *ASCA* days the underlying ionizing continuum of AGN was often mod-

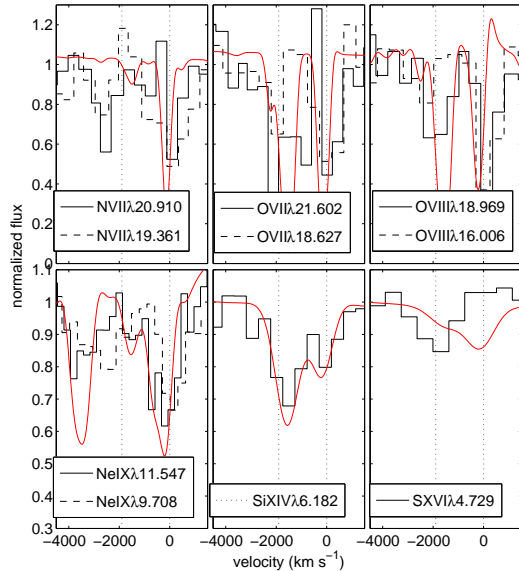


FIG. 15.— Individual line profiles observed in MCG-6-30-15. There is clear evidence for a two component absorption in the spectrum with dotted lines serving as guide lines to their velocities (Sako et al. 2001). Also, more highly ionized lines tend to have a more substantial optical depth at the high velocity end. The red curve shows the specific line profile predictions of our spectral model to the broad-band X-ray spectrum of this source (see text and figure 17).

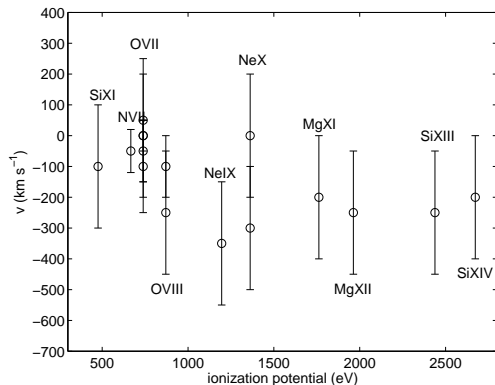


FIG. 16.— Line velocity vs. ionization potential as measured from *Chandra* spectrum of MCG-6-30-15 for the low velocity component of the flow (the high velocity component is not identified in all lines and is not shown). As in all other cases, there is no statistically significant trend detected between the quantities.

eled by a single powerlaw, accumulating *Chandra* and *XMM* observations have shown that this is not the case (e.g., Netzer et al. 2003, Page et al. 2004). For NGC 3783 a soft excess is clearly visible despite the complicated soft X-ray absorption. Other objects, for which absorption is less important, show that, at least in some cases, there is strong evidence for an X-ray hump at soft energies (e.g., Turner et al. 2001, Ogle et al. 2004, Vaughan et al. 2004). The underlying physical mechanism for the soft X-ray hump or excess is unknown and may be related to the accretion disk (e.g., Wang & Netzer 2003), relativistic soft X-ray emission lines (e.g., Branduardi-Raymont et al. 2001), a blend of soft X-ray emission lines (e.g., Pounds et al. 2005), or relativistically smeared absorption (Gierliński & Done 2004). While all of the above applies

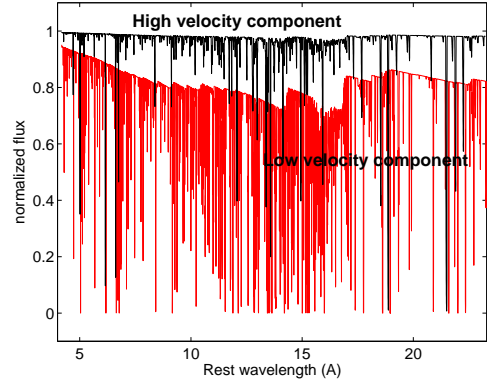


FIG. 17.— The contribution of the low (red curve) and high (black curve) velocity flows to the opacity of the HIG. Note the low opacity of the high velocity component relative to the low velocity component which leads us to conclude that location estimates based on column density considerations alone could be misleading (see text).

to some extent to all AGN, the case of MCG-6-30-15 seems to be unique in the sense that the soft X-ray spectrum is poorly understood, with recent works attempting to explain it as either due to relativistic line emission (e.g., Sako et al. 2003) or dust-related absorption features (e.g., Lee et al. 2001, Ballantyne et al. 2003).

Given the aforementioned uncertainties concerning the X-ray continuum shape at soft X-ray energies we concentrate in this work on the hard X-ray continuum only and note that a well constrained solution may be obtained by fitting for the silicon and sulphur inner shell lines near 6\AA (CN05, N03). For this purpose we have analyzed the recent *Chandra*/HETG observations and confirm the existence of two kinematical components (Sako et al. 2003) that are shown in figure 15. Like in NGC 3783, there is no clear correlation between the ionization level and the velocity of the slower component of the flow (figure 16). Furthermore, the hint for higher ionization levels having somewhat higher outflow velocities is evident from figure 15 where the slower kinematical component has less opacity at high ionization levels. We note that not all lines show clear signature for a high velocity component which is best visible in the O VII, O VIII, and Si XIV lines. In fact, some lines do not show the high velocity component as is evident from figures 1 & 15. We note that high ionization lines (e.g., Si XIV and S XVI tend to have stronger absorption at higher velocities and are consistent with being related to the high velocity component. Judging by the relative strength of higher order resonance transitions it seems that the high velocity flow component has an overall lower column density. We have searched for the existence of the two component flow in the UV band but the poor quality of the IUE data precludes a definite answer to this question (e.g., Reynolds et al. 1997).

It turns out that the physics of the two component outflow cannot be easily explained in the framework of a single outflow model discussed here. One of the problems relates to the lack of significant absorption by high ionization lines at low velocities (e.g., the S XVII $\lambda 4.729$; see figure 15). As discussed here and in CN05, lines coming from the same flow are likely to have very similar line profiles, this was actually the motivation behind the model for the outflow in NGC 3783 (CN05). To reach a velocity of order 2000 km s^{-1} in thermally driven isothermal flows, the sonic velocity should be roughly 400 km s^{-1} ; i.e., corresponding to highly ionized gas at very high temperatures. Thus, if the low velocity compo-

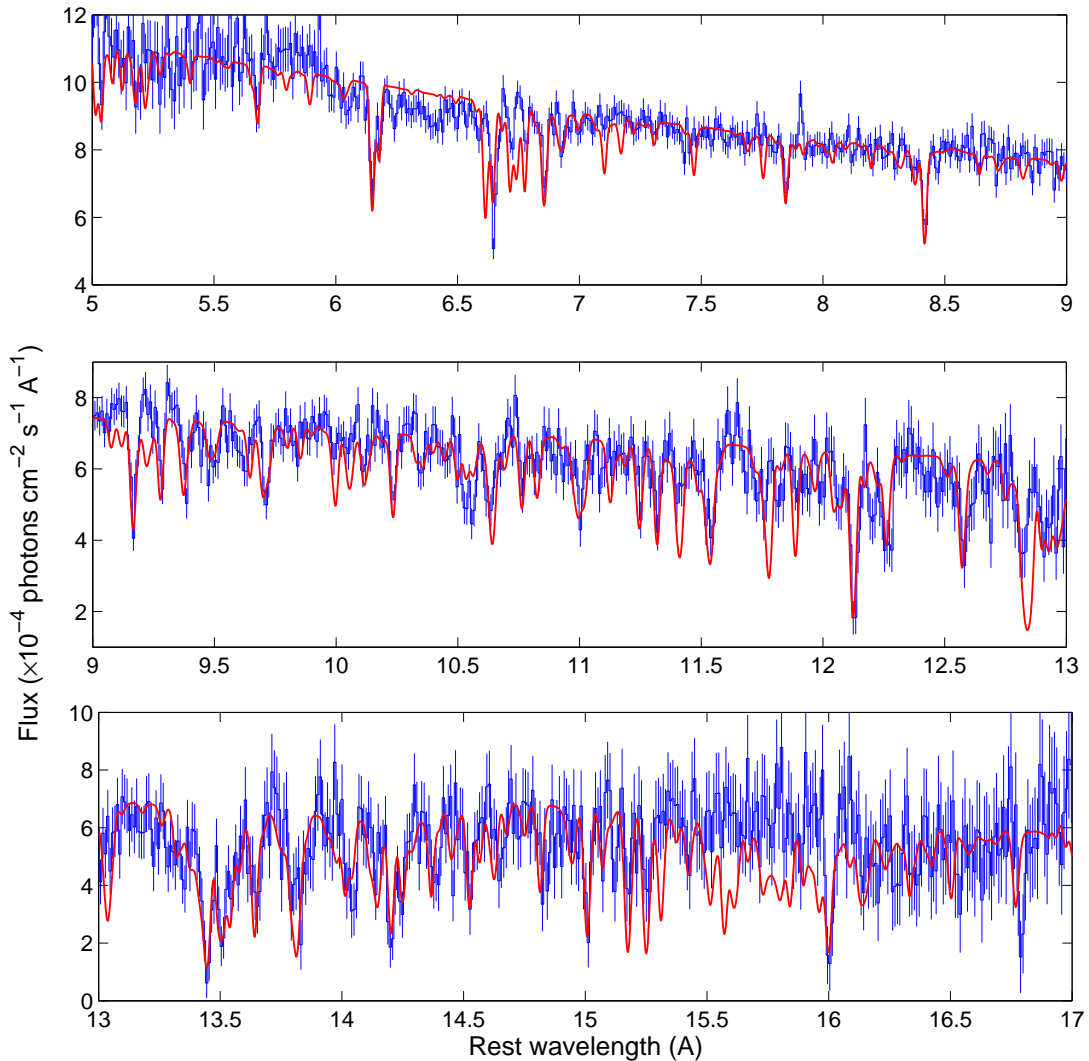


FIG. 18.— An HIG outflow model overlaid on the *Chandra*/HETG spectra of MCG-6-30-15. Clearly, the model reproduces most of the absorption line features as well as the overall shape of the continuum. Some residuals near 15Å are likely due to uncertainties in the di-electronic recombination coefficients of iron (e.g., Netzer 2004).

ment is part of the high velocity flow then it lies in the subsonic region. Such region is likely to be very optically thick (see §4.2) which is not the case here. In addition, to explain the velocity range devoid of any absorption, it is required that the gas be transparent at those velocities; either due to the lack of relatively cold, hence observable gas or due to the lack of gas altogether. In the latter case, the flow cannot be considered as a single entity and the simplified equation of motion used here does not hold. Also, the lack of significant high ionization absorption across the entire velocity range occupied by the two components strongly suggests they are indeed distinct physical components.

It is worth noting that if, as suggested by some authors, the outflowing gas is dusty then its kinematics may be very different than assumed here (since dust particles have a large cross-section for the absorption and scattering of radiation) and could alter our results (e.g., Everett 2002). That said, the lack of conclusive evidence for the existence of dust in this

object and in other objects in our sample, lead us to neglect its effect in the current study. This supports the claim by Ballantyne et al. (2003) stating that dust, if present, is likely to be associated with much larger scales.

In what follows we therefore assume that the two components belong to two different flows or streams and model those accordingly. We first fit the low velocity components which seem to be responsible for most of the X-ray opacity (see above), and then add the high velocity flow component. We assume that both components of the outflow completely cover the ionizing source. The two component model is shown in figure 17 and the model parameters given in table 2. We note that the high velocity flow is relatively optically thin and therefore continuum shielding by it is negligible. The high-velocity model requires an additional heating source apart from photoionization to overcome the effects of adiabatic cooling and drive the flow to the observed velocities. This is not the case for the low velocity component where equally good fits

are obtained in either case (i.e., with and without additional heating source). Our best fit model is shown in figure 18 for which an underlying canonical photon powerlaw of 1.6 has been assumed. While the model does have considerable deviations near 16\AA (probably due to the atomic uncertainties discussed above), the overall agreement is satisfactory. A zoom in on individual lines is shown in figure 15 where the model provides a reasonable fit for most lines with the exception of S XVI $\lambda 4.729$ for which it over-estimates the opacity at the low velocity end.

We emphasize again that we have made no attempt to model the soft X-ray spectrum of this object, despite the good S/N, since our understanding of the various soft X-ray emission components in AGN is limited with MCG-6-30-15 being perhaps a more extreme manifestation of that problem.

While the flows are not co-spatial (the higher velocity stream is launched from roughly an order of magnitude closer in to the ionizing source) interaction between the different streams might occur. The detailed modeling of which is beyond the scope of this paper and requires detailed numerical calculations combining detailed atomic physics and hydrodynamic calculations.

5. DISCUSSION

The purpose of this paper is to determine the mass loss rate and kinetic luminosities associated with outflows in AGN. While similar studies have been possible for stars in which many absorption lines are visible against the ionizing continuum, in AGN there are much fewer lines (essentially none in the optical and only handful in the UV) and the ionizing continuum extends from the UV to the X-rays where many resonance lines are present. For this reason, high resolution, good S/N X-ray spectroscopy is crucial for understanding the dynamics of such flows in those objects.

The main advantage of the model presented here over other methods in the literature is its ability to provide a more physical rather than phenomenological understanding of photoionized flows. It is not the purpose of this paper to provide the best possible fit to the data by a χ^2 standard. While such a method has proven adequate for low resolution CCD spectra, it was shown to be inadequate to model the high-resolution, rich spectra of AGN (N03). Furthermore, obtaining good fits to the data has been successfully done by using pure photoionization models. In particular, for the case of NGC 3783 a three-zone model has been suggested by N03 with 12 free parameters (a column density, ionization parameter, global covering factor of the ionizing source, and an outflow velocity for each zone). While providing a good fit to the absorption spectrum, this method cannot be used to determine the density or distance of the gas from the ionizing source (unless variability arguments are used) and the mass loss rate and kinetic luminosities are essentially undetermined. Contrary to that, only five parameters are used in this work ($U_{\text{ox}}^{\text{min}}$, $U_{\text{ox}}^{\text{max}}$, β , r_0 and C_{global}) that determine not only the thermal and ionization properties of the flow but also its kinematic properties revealing its location, mass loss rate, and kinetic luminosity.

All AGN in our sample show evidence for very highly ionized gas outflowing from their centers. Such gas would have eluded detection by previous X-ray missions and suggests that either such outflows are common in AGN or that they are associated with much cooler gas (e.g., the warm absorber) in those objects. All flows are consistent with a picture in which the gas is multi-phased with higher ionization more dilute phases filling most of the volume. Our best-fit model

parameters for flows in different objects seem to converge to similar values implying similar physics for the HIG in different objects. The flows studied here are thermally driven with radiation pressure force being negligible but in objects shining close to their Eddington luminosity.

Our study shows that, despite the very different manifestations of HIG flows in AGN (e.g., some being more optically thick or having higher velocities than others), the microphysics of all flows is remarkably similar. For example, the wind is multiphase spanning some three orders of magnitude in density at any location with a similar density-scale powerlaw dependence (i.e., similar β). Our analysis also suggests that in objects that shine much below their Eddington rate, and whose wind velocity exceeds $\sim 1000 \text{ km s}^{-1}$, an additional heating source is probably required to balance the effect of adiabatic cooling. (There are several possible such heating mechanism among which is by acoustic waves which are emitted by the cool phase of the gas as it reacts to flux variations of the ionizing source; see Chelouche 2007.) This uniformity of the outflow properties between very different objects is not unexpected since the microphysics of the gas is unlikely to be considerably affected by the macro-physics of the AGN. In fact, this adds credibility to the model in the sense that consistent results are obtained for all objects despite their very different spectra. Furthermore, the value for the ionization parameter at the critical point (derived from table 2) seems to be similar for most objects in our sample. In cases where the flow is more optically thick (e.g., in NGC 4151), the measured velocity is low and our model suggests we may be looking deeper towards the footpoint of the flow. Thus, if our model is correct then it seems that the geometry of the outflowing gas plays a role in the spectral manifestation of type-I objects. This conjecture, however, is based on a handful of objects and is yet to be confirmed observationally and better modeled, theoretically (we note that for thermal driven flows, the notion of stream bending as is the case for radiation pressure driven flows; e.g., Pereyra et al. 1997).

Our results concerning the launching radius of the flow - which we identify with $r_c \sim 1 \text{ pc}$ - is much larger than the size of the inner accretion disk in those objects. This disagrees with some versions of the AGN unification scheme, which suggest that such flows are launched from very close to the black hole in those systems (e.g., Elvis 2000). As discussed in CN05, a promising mass reservoir for these outflows is the putative torus that is thought to lie on scales similar to r_c . Alternative explanations may involve association with the central star cluster. For one object in our sample (NGC 4151; see §4.2) it seems that the outflowing gas obscures the emission region of the iron $K\alpha$ line whose EW is similar to that of typical, non-obscured, type-I sources. Thus, the HIG absorber seems to lie farther out beyond the iron $K\alpha$ emitting region, which is usually identified with the torus (e.g., Netzer et al. 2002). This leads us to conclude that absorption by highly ionized outflows is unlikely to be the cause for obscuration in type-II AGN.

The results regarding the emission from such winds indicate that the global covering fraction is consistent with being of order unity but can be much smaller than that if part of the emission comes from different regions not associated with the flow (as is the case for NGC 4151; Ogle et al. 2004). An extensive study of the possible contributors to the emission spectrum in type-I and type-II objects is beyond the scope of this paper.

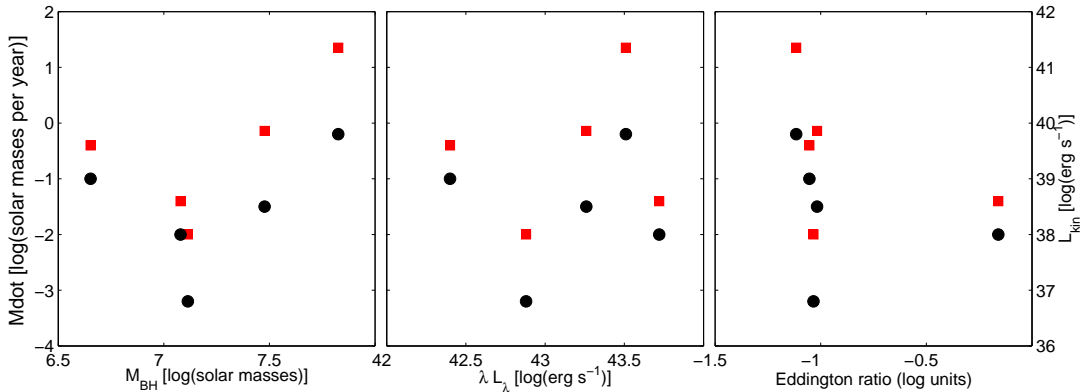


FIG. 19.— Derived mass loss rates (black symbols) and kinetic luminosities (red symbols) as a function of the black hole mass (left panel), optical luminosity (middle panel), and the estimated Eddington ratio (right panel). The kinetic luminosity was calculated using the average velocity of the unblended lines shown in figures 7, 10, 13, & 16 (for NGC 3783 we have used the Kaspi et al. (2002) measurements). There is a hint for a trend where more massive and more luminous objects tend to have more massive and more energetic outflows. We do caution the reader that the mass loss rate has a typical uncertainty of 0.5 dex (not shown, see table 2). In addition, objects with similar emission efficiencies can have very different mass loss rates and kinetic luminosities.

The deduced mass loss rates from AGN indicate that they are roughly of the order of the mass accretion rate yet with a large scatter (see table 2). Thus, to maintain persistent accretion over the AGN lifetime, a large gas reservoir is needed or else a large deposition of matter into the central regions of the galaxy. As the flow velocities are much smaller than the speed of light, the associated kinetic luminosities are very small (typically much less than 0.1%) compared to the bolometric one. The large scatter in the deduced mass loss rate and kinetic luminosity can be traced to the typical velocity of the outflow which varies by a factor of several among objects. This large scatter may be reduced if the true outflow velocity is similar in different objects while the observed velocity is subject to inclination effects. While theoretically plausible, there is no observational support for such a claim and we do not discuss it any further in this work.

Given our results for the mass loss rate and kinetic luminosity of flows we have searched for trends between those quantities and other properties of the AGN. These are shown in figure 19. We do not find any significant correlation between the mass loss rate, \dot{M} , or the kinetic luminosity, L_{kin} and the object’s luminosity, black-hole mass, or the Eddington ratio. There may be a hint for a trend between \dot{M} and L_{kin} and the black hole mass and luminosity which may be driven, in part, by the possible trend between black hole mass and flow velocity (see figure 1).

Extending the diagrams beyond the narrow luminosity range reported here requires detailed observations of more distant quasars as well as low luminosity AGN. It is not at all clear what the spectral signatures from such HIG flows, if at all present, would be in those objects. Nevertheless, for the sake of (perhaps unjustified) simplicity, let us assume that the general properties of the model hold also at higher luminosities and more massive objects. Let us further assume that we increase the object luminosity, L , and black hole mass, M_{BH} in the same proportion so as to maintain a fixed L/L_{Edd} . In this case, for a fixed ionization parameter, the density would scale as L/M_{BH}^2 . Thus, the column density $n\tau \propto L/M_{\text{BH}} \propto L/L_{\text{Edd}} = \text{const.}$ and similar gas opacity, hence absorption features, are expected to occur also in more and less luminous objects for a fixed Eddington rate. The mass loss rate as well as the kinetic luminosity would then be proportional to M_{BH} (or L). Thus, if our model can be extended to high luminosity objects and such objects emit at the same

Eddington ratio as Seyfert galaxies one naively expect the kinetic luminosity to be a constant fraction of the bolometric luminosity (i.e., much less than one per cent). Di Matteo et al. (2005) assumed in their simulations that $L_{\text{kin}}/L \simeq 5\%$, i.e., much larger than the estimates given here. Thus, if our conclusions for the relative kinetic luminosity hold also for highly luminous quasars then such flows cannot account for the necessary feedback effect.

Lastly we note that our spectral fits point to a canonical X-ray spectrum for AGN accreting at sub-Eddington rates in which the hard photon X-ray slope is ~ 1.6 and that any apparent changes to this slope are due to absorption effects. In the soft X-rays there is evidence for a soft excess in some but not all objects, the physical nature of which is currently unclear. The spectral slope is more steep for the one object in our sample which seems to accrete near its Eddington rate. We caution, however, that despite the high quality spectrum and the detailed analysis presented here these conclusions are based on a handful of objects and a more detailed investigation of the complex soft X-ray spectrum is needed to address these issues.

6. CONCLUSION & SUMMARY

We present the first systematic study of type-I AGN with high resolution spectroscopic X-ray observations. Our sample consists of five objects for which good signal-to-noise *Chandra*/*HETG* data are available. We report on our findings concerning the physical properties of highly ionized, low velocity gas seen to be outflowing from those systems. Using a novel scheme for the calculation of the spectral features from thermally and radiatively driven winds we are able to constrain, for the first time, physical properties of the ejected gas pertaining to its location, the mass loss rate, and the associated kinetic luminosity. In addition, the number of free parameters in our model is typically much smaller than that used by pure photoionization models. We find that all AGN in our sample possess highly ionized outflows whose mass loss rate is, on average, of order of the mass accretion (but with a scatter of order a few around this value) while the kinetic luminosity is only a small fraction (typically $\ll 1\%$) of the bolometric luminosity. If this scaling persists to highly luminous quasars then low velocity flows are unlikely to lead to substantial feedback effects. Our results indicate that such flows show an interesting physical similarity among outflows in different objects

suggesting that the gas microphysics in those systems is essentially the same. Different manifestation of such flows can be attributed, at least in part, to geometrical effects. Furthermore, we find that these flows are launched from parsec scales and are unlikely to be associated with the inner parts of the accretion disk. Our study demonstrates the importance of high resolution and S/N X-ray grating observations for understand-

ing the physics of AGN flows.

We thank S. Kaspi for his invaluable help in dealing with the X-ray spectra of NGC 5548 and H. Netzer for helpful comments.

REFERENCES

- Arav, N., Li, Z., & Begelman, M. C. 1994, *ApJ*, 432, 62
 Arav, N. 1996, *ApJ*, 465, 617
 Arav, N., et al. 2007, *ApJ*, 658, 829
 Ballantyne, D. R., Weingartner, J. C., & Murray, N. 2003, *A&A*, 409, 503
 Begelman, M. C., McKee, C. F., & Shields, G. A. 1983, *ApJ*, 271, 70
 Behar, E., Rasmussen, A. P., Blustin, A. J., Sako, M., Kahn, S. M., Kaastra, J. S., Branduardi-Raymont, G., & Steenbrugge, K. C. 2003, *ApJ*, 598, 232
 Blustin, A. J., Page, M. J., Fuerst, S. V., Branduardi-Raymont, G., & Ashton, C. E. 2005, *A&A*, 431, 111
 Blustin, A. J., et al. 2007, *A&A*, 466, 107
 Bonilha, J. R. M., Ferch, R., Salpeter, E. E., Slater, G., & Noerdlinger, P. D. 1979, *ApJ*, 233, 649
 Branduardi-Raymont, G., Sako, M., Kahn, S. M., Brinkman, A. C., Kaastra, J. S., & Page, M. J. 2001, *A&A*, 365, L140
 Chakravorty, S., Kembhavi, A. K., Elvis, M., & Ferland, G. 2008, *arXiv:0811.2404*
 Chelouche, D. & Netzer, H. 2003, *MNRAS*, 344, 223
 Chelouche, D., & Netzer, H. 2005, *ApJ*, 625, 95 (CN05)
 Chelouche, D. 2007, *ApJ* in press (*arXiv:0708.0313*)
 Chevallier, L., Czerny, B., Rózańska, A., & Gonçalves, A. C. 2007, *A&A*, 467, 971
 Chiang, J., & Blaes, O. 2003, *ApJ*, 586, 97
 Crenshaw, D. M., Kraemer, S. B., Boggess, A., Maran, S. P., Mushotzky, R. F., & Wu, C. 1999, *ApJ*, 516, 750
 Di Matteo, T., Springel, V., & Hernquist, L. 2005, *Nature*, 433, 604
 Dorodnitsyn, A., Kallman, T., & Proga, D. 2008a, *ApJ*, 675, L5
 Dorodnitsyn, A., Kallman, T., & Proga, D. 2008b, *ApJ*, 687, 97
 Everett, J., 2002, Ph.D. thesis (*astro-ph/0212421*)
 Everett, J. E., & Murray, N. 2007, *ApJ*, 656, 93
 George, I. M., Turner, T. J., Netzer, H., Nandra, K., Mushotzky, R. F., & Yaqoob, T. 1998, *ApJS*, 114, 73
 George, I. M., Turner, T. J., Yaqoob, T., Netzer, H., Laor, A., Mushotzky, R. F., Nandra, K., & Takahashi, T. 2000, *ApJ*, 531, 52
 Gierliński, M., & Done, C. 2004, *MNRAS*, 349, L7
 Gu, M. F., Holczer, T., Behar, E., & Kahn, S. M. 2006, *ApJ*, 641, 1227
 Halpern, J. P. 1984, *ApJ*, 281, 90
 Holczer, T., Behar, E., & Kaspi, S. 2007, *ApJ*, 663, 799
 Kaastra, J. S., Mewe, R., Liedahl, D. A., Komossa, S., & Brinkman, A. C. 2000, *A&A*, 354, L83
 Kaastra, J. S., Steenbrugge, K. C., Raassen, A. J. J., van der Meer, R. L. J., Brinkman, A. C., Liedahl, D. A., Behar, E., & de Rosa, A. 2002, *A&A*, 386, 427
 Kaastra, J. S., et al. 2004, *A&A*, 422, 97
 Kaspi, S., Smith, P. S., Netzer, H., Maoz, D., Jannuzi, B. T., & Givon, U. 2000, *ApJ*, 533, 631
 Kaspi, S., Brandt, W. N., Netzer, H., Sambruna, R., Chartas, G., Garmire, G. P., & Nousek, J. A. 2000, *ApJ*, 535, L17
 Kaspi, S., et al. 2002, *ApJ*, 574, 643
 Kaspi, S., & Behar, E. 2006, *ApJ*, 636, 674
 Kraemer, S. B., et al. 2001, *ApJ*, 551, 671
 Kraemer, S. B. et al. 2005, *ApJ* in press (*astro-ph/0507354*)
 Krolik, J. H., Kriss, G. A., 2001, *ApJ*, 561, 684
 Krongold, Y., Nicastro, F., Brickhouse, N. S., Elvis, M., Liedahl, D. A., & Mathur, S. 2003, *ApJ*, 597, 832
 Krongold, Y., Nicastro, F., Brickhouse, N. S., Elvis, M., & Mathur, S. 2005, *ApJ*, 622, 842
 Krongold, Y., et al. 2009, *ApJ*, 690, 773
 Lamers, H. J. G. L. M. & Cassinelli, J. P. 1999, *Introduction to stellar winds / Henny J.G.L.M. Lamers and Joseph P. Cassinelli*. Cambridge ; New York : Cambridge University Press, 1999. ISBN 0521593980,
 Lee, J. C., Ogle, P. M., Canizares, C. R., Marshall, H. L., Schulz, N. S., Morales, R., Fabian, A. C., & Iwasawa, K. 2001, *ApJ*, 554, L13
 Matsumoto, C., Moore, J. R., Leighly, K. M., Grupe, D., & Wills, B. J. 2004, *Advances in Space Research*, 34, 2566
 McHardy, I. M., Gunn, K. F., Uttley, P., & Goad, M. R. 2005, *MNRAS*, 359, 1469
 McKernan, B., Yaqoob, T., & Reynolds, C. S. 2007, *MNRAS*, 379, 1359
 Nandra, K., Le, T., George, I. M., Edelson, R. A., Mushotzky, R. F., Peterson, B. M., & Turner, T. J. 2000, *ApJ*, 544, 734
 Netzer, H. 1996, *ApJ*, 473, 781
 Netzer, H., et al. 2003, *ApJ*, 599, 933 (N03)
 Netzer, H. 2004, *ApJ*, 604, 551
 Nikolajuk, M., Papadakis, I. E., & Czerny, B. 2004, *MNRAS*, 350, L26
 Ogle, P. M., Mason, K. O., Page, M. J., Salvi, N. J., Cordova, F. A., McHardy, I. M., & Priedhorsky, W. C. 2004, *ApJ*, 606, 151
 Ogle, P. M., Marshall, H. L., Lee, J. C., & Canizares, C. R. 2000, *ApJ*, 545, L81
 Page, K. L., Schartel, N., Turner, M. J. L., & O'Brien, P. T. 2004, *MNRAS*, 352, 523
 Pereyra, N. A., Kallman, T. R., & Blondin, J. M. 1997, *ApJ*, 477, 368
 Perola, G. C., et al. 1982, *MNRAS*, 200, 293
 Perola, G. C., et al. 1986, *ApJ*, 306, 508
 Peterson, B. M., et al. 2004, *ApJ*, 613, 682
 Petrucci, P. O., Maraschi, L., Haardt, F., & Nandra, K. 2004, *A&A*, 413, 477
 Pounds, K. A., Wilkes, B. J., & Page, K. L. 2005, *MNRAS*, 362, 784
 Proga, D., Ostriker, J. P., & Kurosawa, R. 2008, *ApJ*, 676, 101
 Reynolds, C. S., Ward, M. J., Fabian, A. C., & Celotti, A. 1997, *MNRAS*, 291, 403
 Rózańska, A., Goosmann, R., Dumont, A.-M., & Czerny, B. 2006, *A&A*, 452, 1
 Rózańska, A., Kowalska, I., & Gonçalves, A. C. 2008, *A&A*, 487, 895
 Scannapieco, E. & Oh, S. P. 2004, *ApJ* 608, 62
 Schödel, R., Ott, T., Genzel, R., Eckart, E., Mouawad N., & Alexander, T. 2003, *ApJ*, 596, 1015
 Schulz, N. S., Kallman, T. E., Galloway, D. K., & Brandt, W. N. 2008, *ApJ*, 672, 1091
 Schurch, N. J., Warwick, R. S., Griffiths, R. E., & Kahn, S. M. 2004, *MNRAS*, 350, 1
 Steenbrugge, K. C., et al. 2005, *A&A*, 434, 569
 Smith, R. A. N., Page, M. J., & Branduardi-Raymont, G. 2007, *A&A*, 461, 135
 Turner, T. J., et al. 2001, *ApJ*, 548, L13
 Vaughan, S., Fabian, A. C., Ballantyne, D. R., De Rosa, A., Piro, L., & Matt, G. 2004, *MNRAS*, 351, 193
 Wang, J.-M., & Netzer, H. 2003, *A&A*, 398, 927